Extended Bose–Hubbard model with pair hopping on triangular lattice*

Wang Yan-Cheng(王艳成)[a], Zhang Wan-Zhou(张万舟)[b], Shao Hui(邵 慧)[a], and Guo Wen-An(郭文安)[a]†

[a] Physics Department, Beijing Normal University, Beijing 100875, China
[b] College of Physics and Optoelectronics, Taiyuan University of Technology, Taiyuan 030024, China

(Received 7 April 2013; revised manuscript received 22 April 2013)

We study systematically an extended Bose–Hubbard model on the triangular lattice by means of a meanfield method based on the Gutzwiller ansatz. Pair hopping terms are explicitly included and a three-body constraint is applied. The zero-temperature phase diagram and a variety of quantum phase transitions are investigated in great detail. In particular, we show the existence and the stability of the pair supersolid phase.

Keywords: extended Bose–Hubbard model, pair hopping, zero-temperature phase diagram, pair supersolid

PACS: 67.85.Hj, 03.75.–b, 67.80.kb **DOI:** 10.1088/1674-1056/22/9/096702

1. Introduction

The development in experimentally manipulating ultra-cold atoms in an optical lattice has allowed the realization of novel quantum states and quantum phase transitions in strongly correlated systems,[1,2] e.g., a quantum phase transition from a superfluid (SF) to a Mott insulator (MI) has been predicted and observed.[3] The condensation of paired electrons, which provides the basis of the superconductivity of a metallic superconductor, plays an essential role in modern condensed-matter physics. Thus, realizing pairing related novel quantum states in the context of ultra-cold atoms has attracted considerable interest recently, both in theoretical and experimental research.

It has been demonstrated recently that such states can be realized for lattice bosons with attractive on-site interactions, which are stabilized by a three-body constraint.[4–6] The three-body constraint has been realized by large three-body loss processes.[7,8] The system can be mapped onto spin-1 atoms at unit filling.[9] Besides the conventional atomic superfluid (ASF) phase, a pair (dimer) superfluid (PSF) phase consisting of the condensation of boson pairs emerges under the sufficiently strong attraction.[4–6] The PSF state is manifested as a second-order processes of the single-atom hopping in the optical lattice. Various phase transitions among the ASF, MI, and PSF are investigated in great detail.[4–6,10–14] Both the ground-state and the thermal phase diagrams are obtained. However, the single-species pair supersolid (PSS) was not found in the present system when the nearest-neighbor repulsion is included, except for an isolated continuous supersolid at the Dirac point.[4] The three-body constraint and the effective pair hopping make the system resemble hardcore bosons when on-site repulsion U is weak. Thus, the PSS state might suffer from the same instability of the supersolid state (SS) for hardcore bosons on the square lattice.[15,16] The pair supersolid state was predicted only in the system with correlated hopping[17,18] and in the bilayer system.[19]

For hardcore bosons on the triangular lattice, a supersolid state emerges based on an order-by-disorder mechanism, by which a quantum system avoids classical frustration.[20–23] Aiming to realize PSS state, we thus focus on lattice bosons on the triangular optical lattice. The system we considered is an extended Bose–Hubbard model with the three-body constraint $a_i^{\dagger 3} \equiv 0$. The pair-hopping terms are explicitly included.[24–28] The Hamiltonian is

$$H = -t\sum_{\langle i,j\rangle}(a_i^\dagger a_j + a_j^\dagger a_i) - t_{\rm p}\sum_{\langle i,j\rangle}(a_i^\dagger a_i^\dagger a_j a_j + a_j^\dagger a_j^\dagger a_i a_i) + \frac{U}{2}\sum_i n_i(n_i-1) + V\sum_{\langle i,j\rangle} n_i n_j - \mu\sum_i n_i, \quad (1)$$

where $\langle i,j\rangle$ denotes nearest-neighbor sites, $a_i^\dagger(a_i)$ is the boson creation (annihilation) operator at site i, and $n_i = a_i^\dagger a_i$ is the boson number operator; t ($t_{\rm p}$) is the single-atom (pair) hopping amplitude, U is the on-site interaction, μ is the chemical potential, and V is the nearest-neighbor repulsion. Such a system can be realized experimentally for dipolar bosons polarized by an external electric field and confined in an optical lattice.[29] The pure pair hopping limit ($t = 0$) can be realized by a mechanism based on collisions that induce transport.[30,31] At the limit $V = 0$, the system can be realized in an atom–molecule coupling system in a state-dependent optical lattice.[25] A similar effective model of bosons with the three-body constraint can be realized with spin-1 atoms.[9]

In the present work, we systematically study the model by means of the meanfield method based on the Gutzwiller

*Project supported by the National Natural Science Foundation of China (Grant Nos. 11175018 and 11247251).
†Corresponding author. E-mail: waguo@bnu.edu.cn
© 2013 Chinese Physical Society and IOP Publishing Ltd

ansatz.[32–36] The zero-temperature phase diagram of the system is studied in great detail. The existence of the PSS phase at the $t \to 0$ limit is explained by a mapping between the present model and the hardcore bosons on the triangular lattice. We then show that the PSS phase is stable in the presence of small on-site repulsion U and single-atom hopping t.

This rest of the paper is organized as follows. We first discuss the classical limit of model (1) at zero temperature in Section 2. The model shows various solid states, which are the basis to form a pair supersolid state. Then, we describe the mean-field method in Section 3. We present our main results in Section 4. We discuss the noninteracting case ($U = V = 0$) in Section 4.1. For interacting cases we present the zero-temperature phase diagram in the limit of single-atom hopping $t = 0$, focusing on the parameter region where the pair supersolid phase emerges in Section 4.2. We then investigate if the results are stable against putting a finite t/t_p in Section 4.3, in which a more realistic phase diagram is presented. We conclude in Section 5.

2. Classical limit

There are three sublattices A, B, and C in the triangular lattice, as shown in Fig. 1(a). In the classical limit ($t = 0, t_p = 0$) and zero temperature, the energy per unit cell is

$$E_{\triangle} = \frac{U}{2}[n_A(n_A-1)+n_B(n_B-1)+n_C(n_C-1)] - \mu(n_A+n_B+n_C)+\frac{zV}{2}(n_An_B+n_Bn_C+n_Cn_A), \quad (2)$$

where $z = 6$ is the coordination number of the triangular lattice. n_A, n_B, n_C are the occupation numbers on the sublattices $i =$ A, B, and C, respectively.

A solid state is formed when the symmetry of occupation on the three sublattices is broken spontaneously. The order can be represented by the occupation pattern (n_A, n_B, n_C), with n_A, n_B, n_C not equal. If $n_A = n_B = n_C$, the pattern represents an MI state.

By comparing the energy per unit cell, we obtain the phase boundaries between various ordered phases, as shown in Fig. 1(b). The solid states $(0,0,2)$, $(0,1,2)$, $(0,2,2)$, $(1,1,2)$, and $(1,2,2)$, which have two bosons sitting on one or two sublattices, are of special interest. The corresponding densities are $\rho = 2/3, 1, 4/3, 4/3, 5/3$, respectively. Other solid states related with patterns $(0,0,1), (0,1,1)$ and MI states, $(0,0,0), (1,1,1), (2,2,2)$, with corresponding densities $\rho = 0, 1, 2$, are also found.

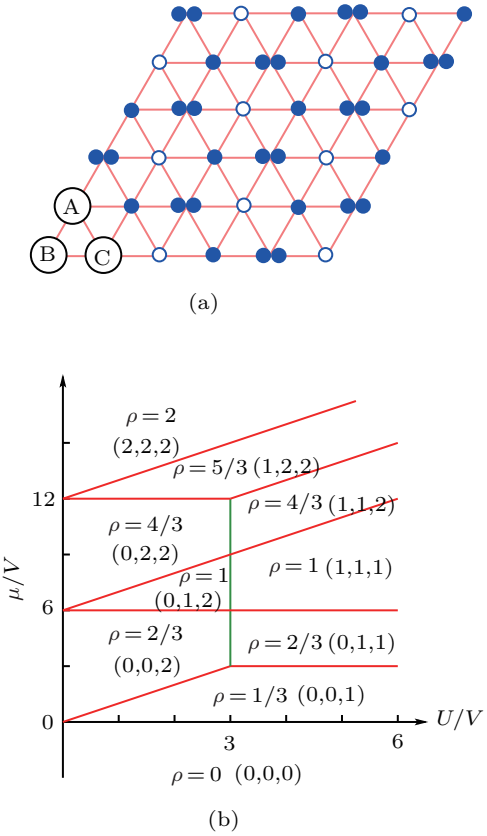


Fig. 1. (color online) (a) The triangular lattice and its three sublattices. The $(0,1,2)$ solid is also shown. (b) Zero-temperature phase diagram in the classical limit $t = 0$, $t_p = 0$.

3. Meanfield method

We start with the Gutzwiller ansatz of the many-body wave function

$$|\psi\rangle = \prod_i \left(\sum_n^{n_{\max}} c_{i,n}|i,n\rangle \right), \quad (3)$$

where $|i,n\rangle$ is the Fock state of n bosons occupying the site i, and $c_{i,n}$ is the probability amplitude. The three-body constraint requires the maximum number of bosons at each site $n_{\max} = 2$. The mean-field decoupling approximation

$$a_i^\dagger a_j = \langle a_i^\dagger\rangle a_j + a_i^\dagger\langle a_j\rangle - \langle a_i^\dagger\rangle\langle a_j\rangle, \quad (4)$$
$$a_i^\dagger a_i^\dagger a_j a_j = \langle a_i^{\dagger 2}\rangle a_j^2 + a_i^{\dagger 2}\langle a_j^2\rangle - \langle a_i^{\dagger 2}\rangle\langle a_j^2\rangle, \quad (5)$$
$$n_i n_j = \langle n_i\rangle n_j + n_i\langle n_j\rangle - \langle n_i\rangle\langle n_j\rangle, \quad (6)$$

are exact for such a state. The atomic superfluid order parameter is defined as $\phi_{a,i} \equiv \langle a_i\rangle = c_{i,0}^* c_{i,1} + \sqrt{2}c_{i,1}^* c_{i,2}$ and the pair superfluid order parameter is $\phi_{p,i} \equiv \langle a_i^2\rangle = \sqrt{2}c_{i,0}^* c_{i,2}$. The average occupancy $\langle n_i\rangle = \sum_n^2 n|c_{i,n}|^2$. For simplicity, we choose the order parameters to be real, i.e., $\phi_{a(p),i} = \phi_{a(p),i}^*$. The mean-field version of the Hamiltonian (1) is thus written as a sum over single-site terms $H = \sum_i H_i$, with

$$H_i = -t(\bar{\phi}_{a,i}a_i^\dagger + \text{H.c.}) - t_p(\bar{\phi}_{p,i}a_i^{\dagger 2} + \text{H.c.})$$

$$+\frac{U}{2}n_i(n_i-1)+V\left(n_i\bar{n}_i-\frac{\langle n_i\rangle\bar{n}_i}{2}\right)-\mu n_i$$
$$+t\bar{\phi}_{\mathrm{a},i}\phi_{\mathrm{a},i}+t_{\mathrm{p}}\bar{\phi}_{\mathrm{p},i}\phi_{\mathrm{p},i}, \tag{7}$$

where $\bar{\phi}_{\mathrm{a(p)},i}=\sum_{\langle j\rangle_i}\phi_{\mathrm{a(p)},j}$ and $\bar{n}_i=\sum_{\langle j\rangle_i}\langle n_j\rangle$ sum over sites j neighboring to site i. Written in the matrix form

$$H_i=\begin{pmatrix} d(0) & -t\bar{\phi}_{\mathrm{a},i} & -\sqrt{2}t_{\mathrm{p}}\bar{\phi}_{\mathrm{p},i} \\ -t\bar{\phi}_{\mathrm{a},i} & d(1) & -\sqrt{2}t\bar{\phi}_{\mathrm{a},i} \\ -\sqrt{2}t_{\mathrm{p}}\bar{\phi}_{\mathrm{p},i} & -\sqrt{2}t\bar{\phi}_{\mathrm{a},i} & d(2)\end{pmatrix}, \tag{8}$$

where the diagonal element

$$d(k)=\frac{U}{2}k(k-1)+V\left(k-\frac{\langle n_i\rangle}{2}\right)\bar{n}_i-\mu k$$
$$+t\bar{\phi}\phi_{\mathrm{a},i}+t_{\mathrm{p}}\bar{\phi}_{\mathrm{p},i}\phi_{\mathrm{p},i}, \tag{9}$$

with $k=0,1,2$.

Without the nearest-neighbor repulsion ($V=0$), there is no solid ordering. The Gutzwiller ansatz (3) reduces to

$$|\psi\rangle=(c_0|0\rangle+c_1|1\rangle+c_2|2\rangle)^N, \tag{10}$$

with N the number of lattice sites. Therefore, $\phi_{\mathrm{a(p)},i}=\phi_{\mathrm{a(p)}},\langle n_i\rangle=\langle n\rangle$, and $\bar{\phi}_{\mathrm{a(p)},i}=z\phi_{\mathrm{a(p)}},\bar{n}_i=z\langle n\rangle$. We then find the ground state in a self-consistent way: Given an initial state $|\psi\rangle$, the order parameters $\phi_{\mathrm{a(p)}}$ and the occupancy $\langle n\rangle$ are calculated. The matrix (8) is thus obtained and diagonalized. $\phi_{\mathrm{a(p)}}$ and $\langle n\rangle$ are then evaluated again from the ground state and put back to Eq. (8). This is done iteratively until the order parameters converge to a self-consistent solution. There can be more than one self-consistent solution. The one with the lowest energy is chosen. This procedure is equivalent to the minimization of the ground energy with respect to the order parameters.[32]

With the nearest-neighbor repulsion ($V\neq 0$) turning on, a solid order may emerge. To accommodate the solid order, we assume

$$|\psi\rangle=\prod_{i=\mathrm{A,B,C}}(c_{i,0}|i,0\rangle+c_{i,1}|i,1\rangle+c_{i,2}|i,2\rangle)^{N_i}, \tag{11}$$

where N_i is the number of sites in sublattice $i\in\mathrm{A,B,C}$. The solid order is represented by the occupation pattern $(\langle n_{\mathrm{A}}\rangle,\langle n_{\mathrm{B}}\rangle,\langle n_{\mathrm{C}}\rangle)$, which can be depicted by a solid order parameter $\Delta\rho^2\equiv\sum_i(\langle n_i\rangle-\rho)^2$, with $\rho=(\sum_i\langle n_i\rangle)/3$ the density of bosons. For a site in sublattice A, one has

$$\bar{\phi}_{\mathrm{a(p)},\mathrm{A}}=\frac{z}{2}(\phi_{\mathrm{a(p)},\mathrm{B}}+\phi_{\mathrm{a(p)},\mathrm{C}}),$$
$$\bar{n}_{\mathrm{A}}=\frac{z}{2}(\langle n_{\mathrm{B}}\rangle+\langle n_{\mathrm{C}}\rangle). \tag{12}$$

Their equivalences under cyclic transformation can also be found. The ground state can be found self-consistently. We start with an arbitrary state, from which the parameters $\phi_{\mathrm{a(p)},\mathrm{A}}$, $\phi_{\mathrm{a(p)},\mathrm{B}}$, $\phi_{\mathrm{a(p)},\mathrm{C}}$, $\langle n_{\mathrm{A}}\rangle$, $\langle n_{\mathrm{B}}\rangle$, and $\langle n_{\mathrm{C}}\rangle$ are evaluated. The matrix (8) for sublattice A is first obtained and diagonalized. From the obtained ground state, "new" $\phi_{\mathrm{a(p)},\mathrm{A}}$ and $\langle n_{\mathrm{A}}\rangle$ are calculated. Then the matrix (8) for sublattice B is obtained and diagonalized. "new" $\phi_{\mathrm{a(p)},\mathrm{B}}$ and $\langle n_{\mathrm{B}}\rangle$ are obtained and used in the matrix (8) for sublattice C. This is done recursively, until the estimated order parameters and occupancies converge. Again, the lowest energy solution is chosen.

The zero-temperature phase diagram of the system is constructed by checking the obtained solutions. The MI and solid states are characterized by $\phi_{\mathrm{a}}=\phi_{\mathrm{p}}=0$, and $\Delta\rho^2=0$ and $\Delta\rho^2\neq 0$, respectively. The ASF and atomic super-solid (ASS) phases are characterized by $\phi_{\mathrm{a}}\neq 0,\phi_{\mathrm{p}}\neq 0$, and $\Delta\rho^2=0$ and $\Delta\rho^2\neq 0$, respectively. The PSF and PSS both have the pair superfluid characters $\phi_{\mathrm{a}}=0$ and $\phi_{\mathrm{p}}\neq 0$. $\Delta\rho^2=0$ in the PSF state, but $\Delta\rho^2\neq 0$ in the PSS phase. In the PSS state, $\phi_{\mathrm{p,A}},\phi_{\mathrm{p,B}}$, and $\phi_{\mathrm{p,C}}$ are different in general. We take the mean value $\phi_{\mathrm{p}}\equiv\sum_i\phi_{\mathrm{p},i}/3$ as the order parameter.

4. Results

In this section, we present our main results.

4.1. Competition between t and t_{p} in the non-interacting case

We start with the non-interacting limit, focusing on the competition between the single-atom hopping t and the pair hopping t_{p}. Without U and V, the diagonal element (Eq. (9)) further reduces to

$$d(k)=-\mu k+zt\phi_{\mathrm{a}}^2+zt_{\mathrm{p}}\phi_{\mathrm{p}}^2. \tag{13}$$

The meanfield solutions for various μ/t and t_{p}/t are found in the way described in Section 3 for the $V=0$ case. The phase diagram is constructed by checking the obtained solutions, as shown in Fig. 2(a). There is a $\rho=0$ MI (empty) phase and a $\rho=2$ MI phase at negative and large chemical potentials, respectively. The MI phase is the result of the three-body constraint. At small pair hopping, there is an ASF phase between the empty phase and the MI phase. The transitions between the ASF phase and the two MI phases can be continuous or first order, depending on the ratio t_{p}/t. This is because, in presence of t_{p}, an energy level crossing may preempt the continuous evolving of the ground state. The first-order transition behavior is shown in Fig. 2(b), in which two energy levels cross each other, leading to a discontinuous change of order parameters. Similar MI-ASF transition behaviors are found in the attractive Bose–Hubbard model with three-body constraint.[10] As pair hopping t_{p} becomes large enough, an ASF–PSF transition happens as expected. The transition is found to be first order, or continuous, depending t_{p}/t, as illustrated in Fig. 2(a). Several tricritical points where the jump of order parameters vanishes are found. However, according to Refs. [4] and [11], the

coupling of the Ising order parameter and the Goldstone mode will drive this quantum phase transition to be a weak first-order one through the Coleman–Weinberg mechanism.[37] For such a weak first-order transition the mean-field theory may be not reliable.

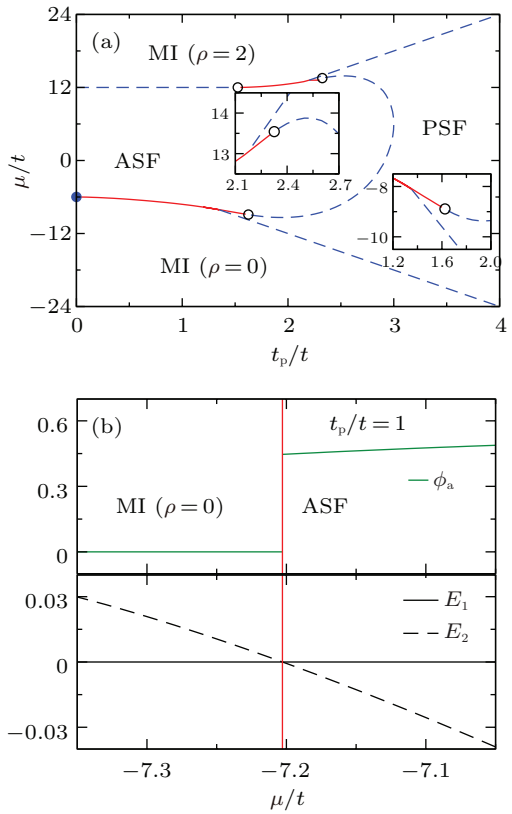


Fig. 2. (color online) (a) Zero-temperature phase diagram at $U=0$, $V=0$. The dashed (blue) lines and the solid (blue) dot represent continuous phase transitions. The solid (red) lines represent the first-order transitions. The open circles denote the tricritical points. The insets show the details around the ASF–PSF tricritical points. (b) Level crossing and the ASF order parameter ϕ_A jump at the MI ($\rho=0$)–ASF transition point, along the $t_p/t=1$ line.

4.2. Limit single-atom hopping $t=0$

We now turn to the interacting case. To demonstrate the effect of the pair hopping term, we first discuss the limit $t=0$, at which equation (8) reduces to

$$H_i=\begin{pmatrix} d(0) & 0 & -\sqrt{2}t_p\bar{\phi}_{p,i} \\ 0 & d(1) & 0 \\ -\sqrt{2}t_p\bar{\phi}_{p,i} & 0 & d(2) \end{pmatrix}, \tag{14}$$

where the diagonal elements read

$$d(k)=\frac{U}{2}k(k-1)+V\left(k-\frac{\langle n_i\rangle}{2}\right)\bar{n}_i-\mu k+t_p\bar{\phi}_{p,i}\phi_{p,i}, \tag{15}$$

with $k=0,1,2$. Without t, the Hamiltonian bears the particle-hole symmetry, which means that it is invariant under the transformation $n\to 2-n$ and $\mu\to 2zV-\mu+U$.

4.2.1. $t=0$, $U\neq 0$, $V=0$

With the on-site repulsion U present the PSF state is the only possible superfluid state and a $\rho=1$ MI state emerges. Without the nearest-neighbor interaction V, no solid order presents. $\phi_{p,i}=\phi_p$ is uniform and $\bar{\phi}_{p_i}=z\phi_p$. Competition between the on-site repulsion and the pair hopping leads to phase transitions among MI and PSF phases.

The diagonal terms in Eq. (14) further reduce to $d(k)=Uk(k-1)/2-\mu k+zt_p\phi_p^2$, and the three eigenvalues are found as follows:

$$\begin{aligned} E_{1,2}&=zt_p\phi_p^2+\frac{U}{2}-\mu\mp\sqrt{\left(\frac{U}{2}-\mu\right)^2+2(zt_p)^2\phi_p^2}, \\ E_3&=zt_p\phi_p^2-\mu, \end{aligned} \tag{16}$$

where E_1 is the ground state if $\mu<0$ or $\mu>U$, considering $U>0$. Note that ϕ_p is self-consistently determined by the eigenvector $v_1=(c_0,0,c_2)$ associated to E_1 as $\phi_p=\sqrt{2}c_2c_0$ and the eigenvector associated to E_3 is $v_3=(0,1,0)$. Given parameters t_p, μ, and U, the self-consistent solution $E_1(\phi_p)$ should satisfy the condition $\partial E_1/\partial\phi_p=0$, which determines the superfluid parameter ϕ_p of the ground state

$$\phi_p=\begin{cases} 0 & \left[\left(\frac{U}{2}-\mu\right)/zt_p\right]^2\geq 1; \\ \frac{1}{2}\sqrt{1-\left[\left(\frac{U}{2}-\mu\right)/zt_p\right]^2} & \left[\left(\frac{U}{2}-\mu\right)/zt_p\right]^2<1. \end{cases} \tag{17}$$

Thus, the PSF and the MI ($\rho=2$) boundary is $\mu/U-1/2=zt_p/U$, where v_1 evolves to (0, 0, 1) and $\phi_p=0$. The PSF and the MI ($\rho=0$) boundary is $\mu/U-1/2=-zt_p/U$, where v_1 evolves to (1, 0, 0) and $\phi_p=0$.

If $0\leq\mu/U\leq 1$, then the eigenlevels E_1 and E_3 may cross each other at the first-order transition point. If both sides of the point have $\phi_p=0$, then $E_1=E_3$ yields $\mu/U=1$, which is the MI ($\rho=1$) and MI ($\rho=2$) transition line, or, $\mu/U=0$, which is the MI ($\rho=1$) and MI ($\rho=0$) transition line. It is still possible that $\phi_p\neq 0$ on one side of the transition and $\phi_p=0$ on the other side, which leads to the following equation:

$$zt_p\phi_p^2+\frac{U}{2}-\mu-\sqrt{(\frac{U}{2}-\mu)^2+2(zt_p)^2\phi_p^2}=-\mu, \tag{18}$$

with $\phi_p\neq 0$ given by Eq. (17). This gives the PSF and MI ($\rho=1$) transition line

$$2zt_p/U=1+\sqrt{1-(2\mu/U-1)^2}. \tag{19}$$

The phase diagram is shown in Fig. 3(a), which can be compared with the similar phase diagram presented in Refs. [25] and [28], where the three-body constraint was not applied. Due to the particle–hole symmetry, the phase diagram is symmetric about $\mu/U=1/2$. The nature of phase transitions involved is further investigated, as illustrated in Fig. 3(b), where μ/U varies from -1 to 2 along the line $t_p/U=0.15$. It is clear that the transitions between the $\rho=0,\rho=2$ MI phases and the PSF phase are continuous, while the transition between

the $\rho = 1$ MI and the PSF is the first-order transtion. The latter behavior is different from the nature of the SF–MI transition in the softcore Bose–Hubbard model with single-atom hopping. The $\rho = 1$ MI state $v_3 = (0,1,0)$ can not evolve to the PSF state v_1 continuously in the truncated Hilbert space due to the three-body constraint.

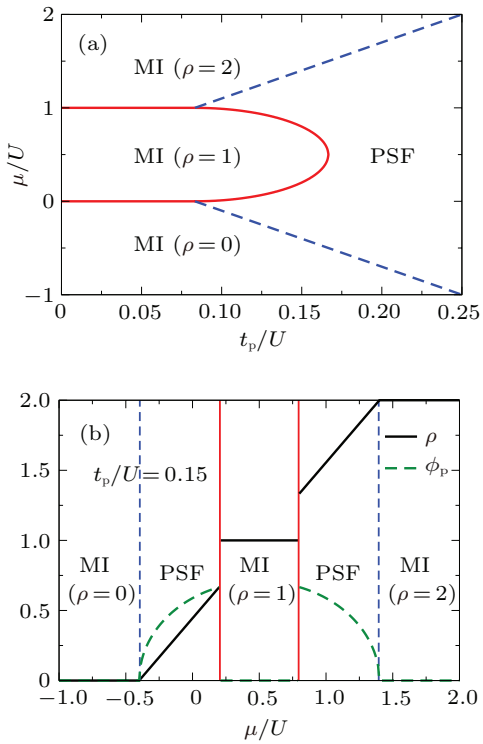


Fig. 3. (color online) (a) Zero-temperature phase diagram at $t = 0$, $V = 0$. The solid (red) lines denote the first-order phase transitions, while the dashed (blue) lines represent continuous phase transitions. (b) Density ρ and pair superfluid parameter ϕ_p versus μ/U at $t_p/U = 0.15$.

4.2.2. $t = 0$, $U = 0$, $V \neq 0$

With the nearest-neighbor interaction V turning on, but the on-site repulsion turning off, two solid phases: (0, 2, 2) and (2, 0, 0), emerge, as shown in Fig. 4. Between the two solids, there are two PSS phases (A and B) which are characterized by local density fluctuations $\Delta\rho \neq 0$ and the mean PSF order parameter $\phi_p \neq 0$ and the ASF order parameter $\phi_a = 0$. The boson density in PSS-A $\rho < 1$, while that in PSS-B $\rho > 1$. The PSF phase exists at the outside of the two solids and the PSS phases, between the empty phase and the $\rho = 2$ MI phase. Due to the particle-hole symmetry, the phase diagram is symmetric about $\mu/V = 6$.

The phase diagram is much like that of the meanfield hardcore Bose–Hubbard model on the triangular lattice.[38] The only difference is that the pair states replace the corresponding single-atom states: the PSS state replaces the ASS state and the PSF state replaces the ASF state. This can be understood in the following way. The matrix of the meanfield Hamiltonian of the hardcore bosons on the triangular lattice is

$$H_i^{(\mathrm{hc})} = \begin{pmatrix} d(0) & -t\bar{\phi}_{a,i} \\ -t\bar{\phi}_{a,i} & d(1) \end{pmatrix}, \tag{20}$$

where the diagonal element is

$$d(k) = V\left(k - \frac{\langle n_i \rangle}{2}\right)\bar{n}_i - \mu k + t\bar{\phi}_{a,i}\phi_{a,i}, \tag{21}$$

with $k = 0, 1$. Considering $U = 0$, the ground state of H_i in Eq. (14) is always in the subspace extended by the two Fork states $|0\rangle$ and $|2\rangle$. The matrix of H_i is thus equivalent to $H_i^{(\mathrm{hc})}$ after applying the mapping $2t_p \to t, 2\mu \to \mu$. The ground state of H_i: $|\psi\rangle_i = c_{i,0}|0\rangle + c_{i,2}|2\rangle$ maps to the ground state of $H_i^{(\mathrm{hc})}$: $|\psi^{(\mathrm{hc})}\rangle_i = c_{i,0}|0\rangle + c_{i,2}|1\rangle$, which leads to $\phi_p = \sqrt{2}\phi_a$, with ϕ_p the PSF order parameter of H_i and ϕ_a the ASF order parameter of hardcore bosons. Therefore, the phase diagram Fig. 4 can be obtained from the meanfield phase diagram of the hardcore bosons on the triangular lattice[38] after applying the mapping.

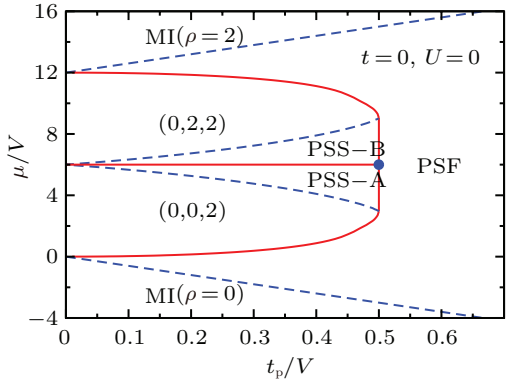


Fig. 4. (color online) Zero-temperature phase diagram at $t = 0, U = 0$. The solid (red) lines denote the first-order phase transitions, while the dashed (blue) lines and the solid (blue) dot represent continuous phase transitions.

The properties of phase transitions are also obtained. Transitions from the PSF to the two solids [(0,0,2) and (0,2,2)], and to the PSS states are first order, except for the $\mu/V = 6$ point marked by a blue dot in Fig. 4, but those from the PSF to the MI phases and from the PSS to the two solids are continuous.[39,40] The transition from PSS-A to PSS-B is first order. These results are consistent with that found for hardcore bosons on the triangular lattice.[21,39,40] In a recent work,[41] a Quantum Monte Carlo study also predicts the PSS phase between the two solids. However, the PSS region is much smaller due to quantum fluctuations.

4.2.3. $t = 0$, $U \neq 0, V \neq 0$

With the on-site repulsion U present, more phases emerge, as shown in Fig. 5. When U/V is not large (< 3.3), the PSS phase persists. In the strength $U/V > 3$, a $\rho = 1$ MI phase (1, 1, 1) emerges and the solid phases (1, 1, 2) and (0, 1, 1) take over the (0, 2, 2) and (0, 0, 2) solids. Nevertheless, as long as $U/V < 3.3$, the pair hopping term can still lower the ground state energy by forming the PSS-A or B states on the basis of (2, 0, 0) or (0, 2, 2) solid, respectively. For example, at $U/V = 3.1, \mu/V = 6, t_p/V = 0.48$, we find the ground state is a PSS-A state

$$|\psi\rangle = (0.353|0\rangle + 0.935|2\rangle)^{N_A}(0.912|0\rangle + 0.409|2\rangle)^{N_B}$$

$$\times (0.912|0\rangle + 0.409|2\rangle)^{N_C}, \quad (22)$$

which leads to the occupancy (1.750, 0.335, 0.335), ASF order parameter $\phi_a = 0$, and the mean PSF order parameter $\phi_p = 0.508$. Above the threshold $U/V = 3.3$, the PSS phases disappear finally. The properties of associated phase transitions are investigated by checking various order parameters, as illustrated in Fig. 5(b), in which various order parameters are plotted as functions of μ/V at $U/V = 2, t_p/V = 0.36$.

4.3. Finite t/t_p in interacting cases

We now turn to discuss if the above results are stable when we put in the single-atom hopping t.

4.3.1. $V = 0,\ U \neq 0$

We first study the change of the phase diagram shown in Fig. 3.

For small enough t, two ASF phases emerge at the boundary of the $\rho = 1$ MI and the $\rho = 2$ MI phases, and at that of the $\rho = 1$ MI and the $\rho = 0$ MI phases, as shown in Fig. 6(a). The MI ($\rho = 2$)–PSF and the MI ($\rho = 0$)–PSF transitions are continuous, while the MI ($\rho = 1$)–PSF transition is still first order. The MI–ASF transitions and the ASF–PSF transition changes from continuous to first order, due to the mechanism that level crossing preempts the continuous evolving, according to our meanfield analysis. Here, the aforementioned coupling of the Ising order parameter and the Goldstone mode may change the phase transition behavior. Further investigation beyonds the mean-field theory is needed.

When t is large enough, the $\rho = 1$ MI phase is excluded by the ASF phase completely, as shown in Fig. 6(b). Quantum hopping dominates the physics. The phase diagram shows the same topology as that for the non-interacting case [Fig. 2(a)].

4.3.2. $U = 0$ but $V \neq 0$

We now check the stability of the phase diagram (Fig. 4) in the presence of the single-atom hopping t.

With small t, an ASF region emerges between the $\rho = 2$ MI and the (0, 2, 2) solid phases, meanwhile, another ASF phase emerges between the $\rho = 0$ MI and the (2, 0, 0) solid phases, as shown in Fig. 7(a). In addition, two ASS phases (A: $\rho < 1$, B: $\rho > 1$) emerge in the PSS region at small t_p/V, between two solid phases. Large PSS region persists in the region with larger t_p/V. The ASS–PSS transition is continuous and the PSS-PSF transition is first order, as illustrated in Fig. 7(b).

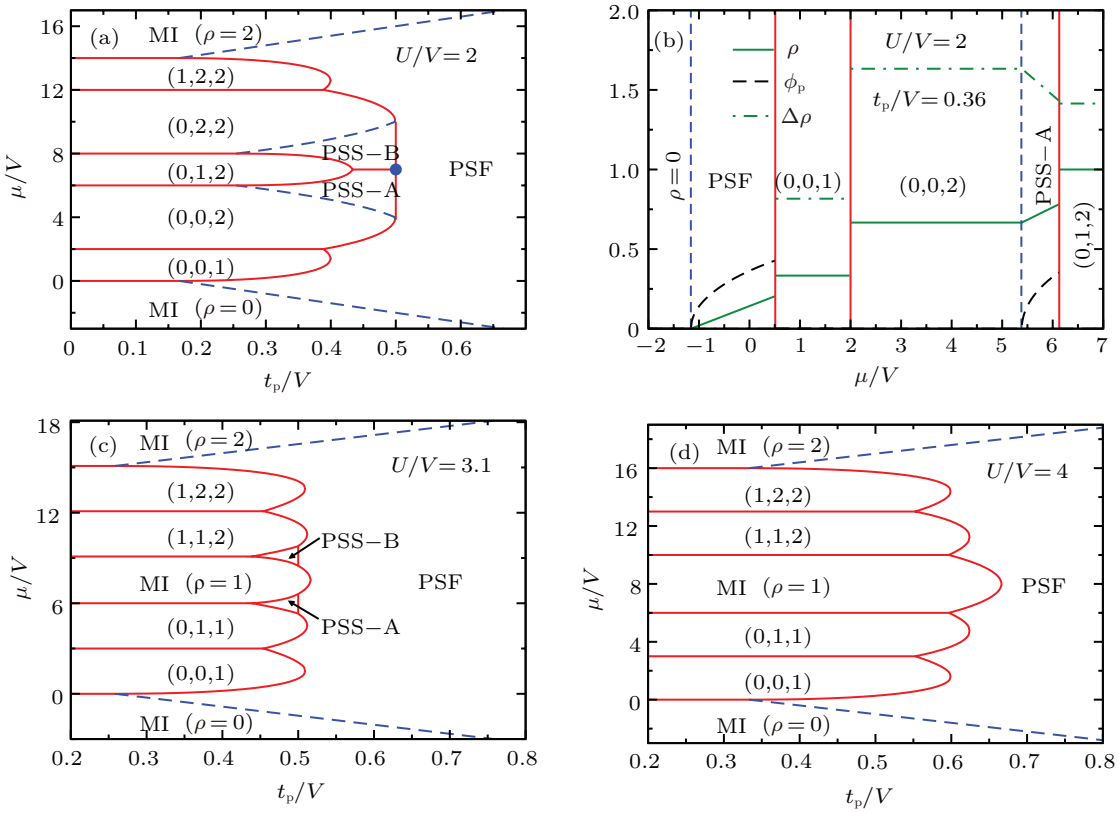


Fig. 5. (color online) (a), (c), (d) Zero-temperature phase diagram for $U/V = 2, 3.1, 4$, respectively. The first-order phase transitions are denoted by solid (red) lines, whereas the continuous phase transitions are represented by dashed (blue) lines and the solid (blue) dot. (b) The density ρ, PSF order parameter ϕ_p, and solid order parameter $\Delta\rho$ versus μ/V at $t_p/V = 0.36$, $U/V = 2$.

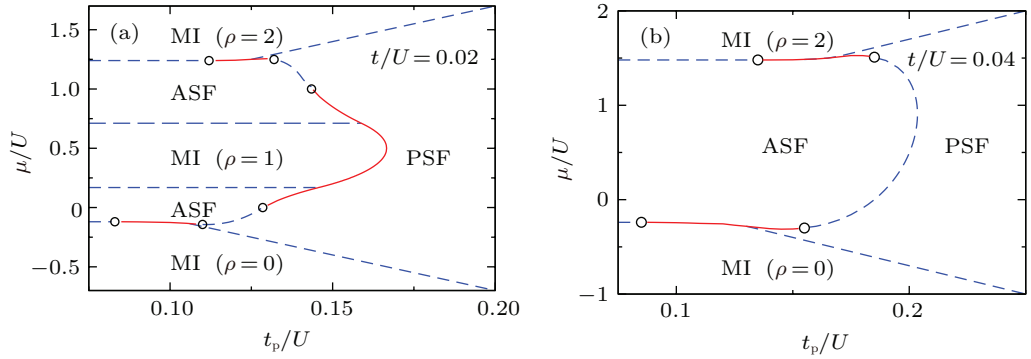


Fig. 6. (color online) Zero-temperature phase diagram for $V=0$ at $t/U=0.02$ (a) and at $t/U=0.04$ (b). The solid (red) line denotes the first-order phase transition, while the dashed (blue) lines represent continuous phase transitions. Open circles denote tricritical points.

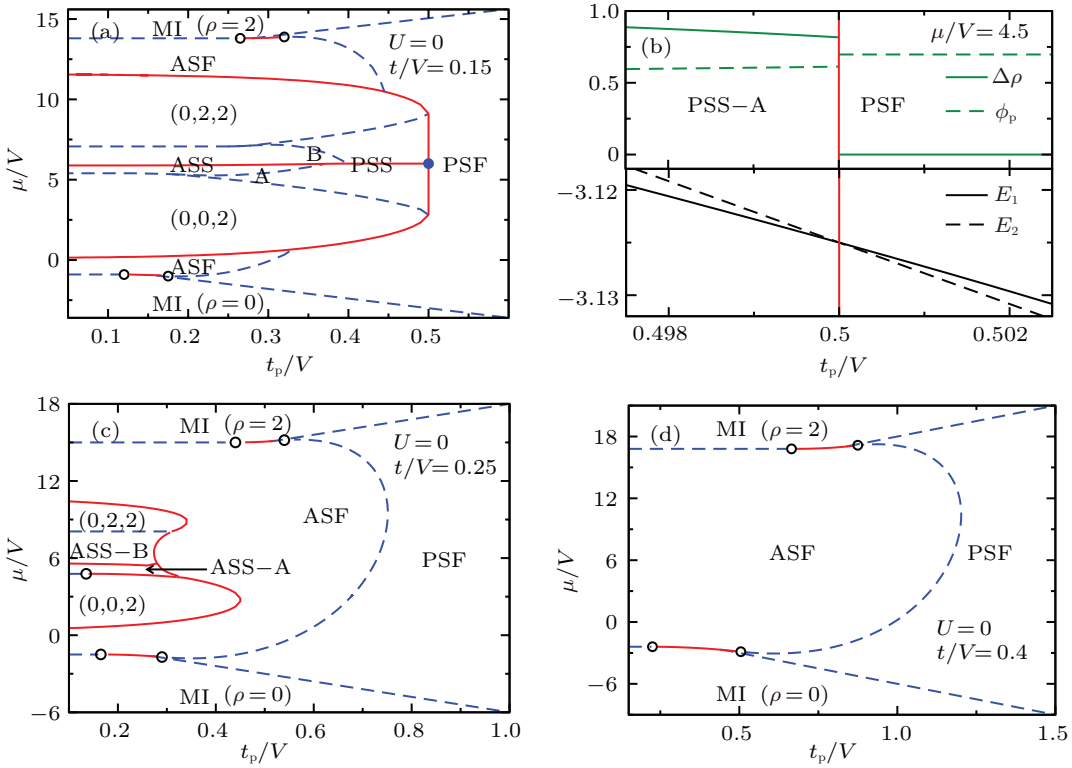


Fig. 7. (color online) Zero-temperature phase diagram at $U=0, t/V=0.15$ (a), $t/V=0.25$ (c) and $t/V=0.4$ (d). The solid (red) lines denote the first-order phase transitions, while the dashed (blue) lines and the solid (blue) point represent continuous phase transitions. The open circles denote tricritical points. Level crossing and the jumps of order parameters of the PSS-A to PSF transition at $\mu/V=4.5$ are shown in (b).

When t becomes larger, the ASF region is enlarged and encloses the solid and the ASS phases, and the PSS phases disappear, as shown in Fig. 7(c). One interesting phenomenon is that the ASS-A to the (0, 0, 2) solid phase changes from first order to continuous when t_p/V is weakened, while the ASS-B to the (0, 2, 2) solid phase is always continuous.

When t becomes even larger, all solid phases and ASS phases disappear. The dominant physics is the ASF–PSF phase transition. The phase diagram for $t/V=0.4$ is presented in Fig. 7(d), showing the same topology as the non-interacting case [Fig. 2(a)].

4.3.3. Both $U\neq 0$ and $V\neq 0$

In a real experimental system, the quantum hoppings and atom interactions can exist simutaneously. The interplay among them results in complex but interesting physics effects. We fix the ratios $\mu/V=5.8$ and $t_p/t=5$ and show the zero-temperature phase diagram in the parameter space t_p/V and U/V, see Fig. 8(a).

When the nearest-neighbor repulsion V dominants, the system is in the (0, 0, 2) solid phase. As hopping strength grows, the system goes to the PSS-A state through a continuous phase transition. Further enlarging the hopping strength results in the PSF state through a first-order transition. The PSS-A phase is stabilized in a large parameter region.

On the other hand, the system is in the (0, 1, 1) solid state if the on-site repulsion U dominants. As hopping strength increases, the system undergoes a continuous transition to the ASS-B phase. By increasing further the hopping strength, the solid order is destroyed and bosons undergo a first-order tran-

sition to the ASF phase. Even larger hopping with the fixed ratio $t_p/t = 5$ drives the system into the PSF phase through a continuous transition, as expected.

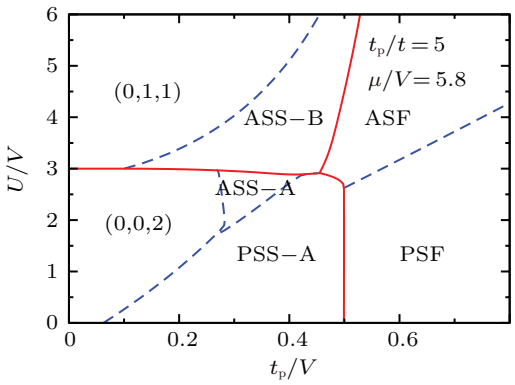


Fig. 8. (color online) Zero-temperature phase diagram at $t_p/t = 5$, $\mu/V = 5.8$. The solid (red) lines denote the first-order phase transitions, while the dashed (blue) lines represent continuous phase transitions.

In the middle values of U/V and t_p/V, a small region of ASS-A phase exists.

5. Conclusion

We have studied systematically the extended Bose–Hubbard model on the triangular lattice, in which the pair hopping terms are explicitly included and the three-body constraint is applied, by means of mean-field approaches based on the Gutzwiller ansatz. The zero-temperature phase diagram and various quantum phase transitions are investigated in great detail. In particular, the existence and stability of the pair supersolid phases are shown. At the limit that the single-atom hopping is zero, we provided the mapping between the present model and the hardcore bosons on the triangular lattice. The existence of the PSS phase is thus understood. We have also shown that the PSS phase is stable under the perturbation of the on-site repulsion and the finite single-atom hopping. Experimentally, the triangular optical lattice can be implemented.[42] The three-body constraint can be realized with spin-1 atoms[9] or large three-body loss processes.[7,8] Our results for the pure pair hopping limit ($t = 0$) are applicable to the system in which boson pair hopping is based on collisions that induce transport.[30,31] The results in the parameter space $V = 0$ are applicable to the atom–molecule coupling system proposed in Ref. [25], when the three-body constaint is applied. For $V \neq 0$, our results are useful to analyse dipolar bosons polarized by an external electric field and confined in an optical lattice.[29] However, in such a system, the occupation-dependent single-atom hopping needs to be discussed.

References

[1] Lewenstein M, Sanpera A, Ahufinger V, Damski B, Sen(De) A and Sen U 2007 *Adv. Phys.* **56** 243
[2] Bloch I, Dalibard J and Zwerger W 2008 *Rev. Mod. Phys.* **80** 885
[3] Greiner M, Mandel O, Esslinger T, Hänsch T W and Bloch I 2002 *Nature* **415** 39
[4] Diehl S, Baranov M, Daley A J and Zoller P 2010 *Phys. Rev. Lett.* **104** 165301
[5] Diehl S, Baranov M, Daley A J and Zoller P 2010 *Phys. Rev. B* **82** 064509
[6] Diehl S, Baranov M, Daley A J and Zoller P 2010 *Phys. Rev. B* **82** 064510
[7] Daley A J, Taylor J M, Diehl S, Baranov M and Zoller P 2009 *Phys. Rev. Lett.* **102** 040402
[8] Roncaglia M, Rizzi M and Cirac J I 2010 *Phys. Rev. Lett.* **104** 096803
[9] Mazza L, Rizzi M, Lewenstein M and Cirac J I 2010 *Phys. Rev. A* **82** 043629
[10] Lee Y W and Yang M F 2010 *Phys. Rev. A* **81** 061604
[11] Ng K K and Yang M F 2011 *Phys. Rev. B* **83** 100511
[12] Bonnes L and Wessel S 2011 *Phys. Rev. Lett.* **106** 185302
[13] Chen Y C, Ng K K and Yang M F 2011 *Phys. Rev. B* **84** 092503
[14] Bonnes L and Wessel S 2012 *Phys. Rev. B* **85** 094513
[15] Sengupta P, Pryadko L P, Alet F, Troyer M and Schmid G 2005 *Phys. Rev. Lett.* **94** 207202
[16] Batrouni G G and Scalettar R T 2000 *Phys. Rev. Lett.* **84** 1599
[17] Schmidt K P, Dorier J, Läuchli A and Mila F 2006 *Phys. Rev. B* **74** 174508
[18] Jiang H C, Fu L and Xu C K 2012 *Phys. Rev. B* **86** 045129
[19] Trefzger C, Menotti C and Lewenstein M 2009 *Phys. Rev. Lett.* **103** 035304
[20] Wessel S and Troyer M 2005 *Phys. Rev. Lett.* **95** 127205
[21] Boninsegni M and Prokof'ev N 2005 *Phys. Rev. Lett.* **95** 237204
[22] Melko R G, Paramekanti A, Burkov A A, Vishwanath A, Sheng D N and Balents L 2005 *Phys. Rev. Lett.* **95** 127207
[23] Heidarian D and Damle K 2005 *Phys. Rev. Lett.* **95** 127206
[24] Yang S J 2009 *Commun. Theor. Phys.* **52** 611
[25] Zhou X F, Zhang Y S and Guo G C 2009 *Phys. Rev. A* **80** 013605
[26] Yang S J and Feng S P 2010 *New J. Phys.* **12** 023032
[27] Guo H L, Yin X G and Chen S 2011 *J. Phys. B* **44** 195002
[28] Wang Y M and Liang J Q 2012 *Chin. Phys. B* **21** 060305
[29] Sowiński T, Dutta O, Hauke P, Tagliacozzo L and Lewenstein M 2012 *Phys. Rev. Lett.* **108** 115301
[30] Eckholt M and García-Ripoll J J 2008 *Phys. Rev. A* **77** 063603
[31] Eckholt M and García-Ripoll J J 2009 *New J. Phys.* **11** 093028
[32] Sheshadri K, Krishnamurthy H R, Pandit R and Ramakrishnan T V 1993 *Europhys. Lett.* **22** 257
[33] Jaksch D, Bruder C, Cirac J I, Gardiner C W and Zoller P 1998 *Phys. Rev. Lett.* **81** 3108
[34] Iskin M 2011 *Phys. Rev. A* **83** 051606
[35] Lu X C and Yu Y 2006 *Phys. Rev. A* **74** 063615
[36] Pai R V, Kurdestany J M, Sheshadri K and Pandit R 2012 *Phys. Rev. B* **85** 214524
[37] Coleman S and Weinberg E 1973 *Phys. Rev. D* **7** 1888
[38] Murthy G, Arovas D and Auerbach A 1997 *Phys. Rev. B* **55** 3104
[39] Bonnes L and Wessel S 2011 *Phys. Rev. B* **84** 054510
[40] Yamamoto D, Danshita I and Sá de Melo C A R 2012 *Phys. Rev. A* **85** 021601
[41] Zhang W Z, Wang Y C and Guo W A 2012 arXiv: 1208.6506
[42] Becker C, Soltan-Panahi P, Kronjäger J, Dörscher S, Bongs K and Sengstock K 2010 *New J. Phys.* **12** 065025